Improvement in Abrasion Wear Resistance and Microstructural Changes with Deep Cryogenic Treatment of Austempered Ductile Cast Iron (ADI)

SANJA ŠOLIĆ, MATJAŽ GODEC, ZDRAVKO SCHAUPERL, and ČRTOMIR DONIK

The application of a deep cryogenic treatment during the heat-treatment processes for different types of steels has demonstrated a significant influence on their mechanical and tribological properties. A great deal of research was conducted on steels, as well as on other kinds of materials, such as hard metal, gray cast iron, aluminum, aluminum alloys, *etc.*, but not on austempered ductile iron (ADI). In this research the influence of a deep cryogenic treatment on the microstructure and abrasive wear resistance of austempered ductile iron was investigated. The ductile cast iron was austempered at the upper ausferritic temperature, deep cryogenically treated, and afterwards tempered at two different temperatures. The abrasion wear resistance was tested using the standard ASTM G65 method. The microstructure was characterized using optical microscopy, field-emission scanning electron microscopy, electron back-scattered diffraction, and X-ray diffraction in order to define the microstructural changes that influenced the properties of the ADI. The obtained results show that the deep cryogenic treatment, in combination with different tempering temperatures, affects the matrix microstructure of the austempered ductile iron, which leads to an increase in both the abrasion wear resistance and the hardness.

I. INTRODUCTION

AUSTEMPERED ductile cast iron (ADI) has become an important engineering material in recent years due to its interesting combination of properties, such as very good strength-to-weight ratio, good toughness, high wear resistance, and excellent fatigue strength in combination with the low cost, design flexibility, and good machinability. As a result of these properties, which are a consequence of the ADI's specific microstructure that consists of needle-like bainitic ferrite (α_B) and high-carbon austenite (γ_{HC}),[1–5] ADI is increasingly used in the automotive industry as a substitute for steel and aluminum parts.

Due to the similarity of the heat-treatment procedure and the microstructure when compared with austempered steels, it has wrongly been believed for some time that the microstructure of ADI consists of bainite. This bainite is a low-temperature eutectoid that consists of needle-like ferrite and carbides, while correctly heat-treated ADI has no carbides present in the microstructure. Also, the presence of austenite at room temperature leads to the wrong conclusions, *i.e.*, it is the residual austenite that is equal to the unstable residual austenite present in the steel microstructure after an incomplete heat treatment. The austenite present in the microstructure of ADI is stabilized with carbon enrichment during the heat-treatment process and will, according to some authors, begrudgingly transform to martensite even at subzero temperatures.[6–8]

The heat treatment that results in the ADI's specific ausferritic microstructure involves austenitizing in order to achieve a full austenitic matrix, followed by rapid cooling or quenching to the austempering temperature in order to avoid the formation of pearlite and other high-temperature phase transformations. The austempering temperature, which is in the range between 523 K and 673 K (250 °C and 400 °C), is the most important parameter in the heat-treatment procedure for ADI, because it determines the final microstructure and the properties of the material. With different combinations of the time and the temperature of austenitizing and austempering, it is possible to obtain different combinations of properties that can be specifically designed and adjusted for a certain purpose.

Austempering in the lower-temperature range results in a microstructure of fine-grained, needle-like, or acicular-shaped ferrite and austenite (lower ausferrite) with a higher strength and a lower impact toughness and ductility. Whereas, the higher austempering temperatures result in coarse, feathery ferrite, and austenite (upper ausferrite), which lowers the strength but has a

SANJA ŠOLIĆ and ČRTOMIR DONIK, Senior Research Associates, and MATJAŽ GODEC, Director, are with the Institute for Metals and Technology, Lepi pot 11, 1000 Ljubljana, Slovenia. Contact e-mail: sanja.solic@imt.si ZDRAVKO SCHAUPERL, Full Professor, is with the Faculty for Mechanical Engineering and Naval Architecture, University of Zagreb, I. Lučića 5, 10000 Zagreb, Croatia.

positive impact on the ductility and the toughness of the ADI.[9,10]

During the austempering process ADI goes through two stages. During the first stage the austenite (γ) decomposes into bainitic ferrite (α_B) and high-carbon austenite (γ_{HC}), a microstructure that is also known as ausferrite.[2] If the austempering time is too long, a carbon-enriched austenite will start its subsequent decomposition, in the second stage of the transformation, into ferrite (α_B) and carbides. Transition carbides, like ε-carbides, usually start to form at the beginning of the second-stage transformation and are responsible for the brittleness of the material.[11] With a longer period of time the ε-carbides transform into incoherent Fe_3C[4–6] and the material ends up with a bainitic microstructure. So, the optimum properties for the ADI will be achieved if the austempering period finishes during the first stage. The microstructure of the ADI after a properly conducted austempering process will consist of high-carbon austenite and bainitic ferrite as a matrix around graphite nodules.

A deep cryogenic treatment is a heat-treatment procedure where the material is subjected to subzero temperatures before tempering[12,13] so as to obtain dimensional stability, but also to improve the abrasive, fatigue, and wear resistance.[14–17] In practice there are two subzero temperature ranges. The first is known as a cold treatment or a shallow cryogenic treatment, in the temperature range between 193 K to 153 K (-80 °C to -120 °C) (dry ice), which is enough to transform the retained austenite into martensite in quenched steels. This has wide-ranging commercial applications, especially for the removal of the retained austenite in carburized and surface-hardened steels.[15,18] The second is known as a deep cryogenic treatment, which is performed at temperatures below 77 K (-196 °C) (liquid nitrogen and other liquid gases), and primarily influences the wear resistance of the material. This improvement in properties occurs as a result of the complete transformation of the retained austenite into martensite and the precipitation of ultrafine η-carbides in the tempered martensitic matrix.[15,19–21] Deep cryogenic treatment is currently very popular in research, with reports covering tool steels, maraging steels, cast irons, annealing steels, hard metals, aluminum, and others.[12–26] Despite the very successful results reported for the influence of deep cryogenic treatments on the mechanical and tribological properties of a large number of materials, the use of this process for ADI has not been the topic of much research. One reported study by Putatunda et al.[27] investigated the influence of a deep cryogenic treatment on the mechanical properties of ADI that was austempered in the lower austempering temperature range 561 K (288 °C) and found that the cryogenic treatment influenced the ausferritic microstructure of the ADI and caused the complete transformation of the high-carbon austenite into martensite without any application of mechanical force. A recent study by Panneerselvam et al.[28] investigated the influence of the deep cryogenic treatment of ADI on the stability of high-carbon austenite since it was not clear whether the austenite formed at the lower austempering temperatures is more

mechanically and thermally stable than that produced at the upper austempering ranges. They found that the cryogenic treatment improved the tensile strength and the hardness of the ADI in samples austempered in the range 561 K to 672 K (288 °C to 399 °C), while the elongation was observed to decrease, and the fracture toughness remained unaffected. They also concluded that the austenite formed at the upper austempering temperatures between 644 K and 672 K (371 °C and 399 °C) had a greater degree of thermal stability and was only partially transformed into martensite during the cryogenic treatment.

Several authors have studied ADI's abrasive wear resistance. Zimba et al.[29] investigated the abrasive wear resistance of ADI that was austempered at 648 K (375 °C) with a hardness of 315 HV, comparing it with a quenched-and-tempered steel with a hardness of 635 HV. They concluded that the abrasive wear resistance of ADI is much better than that of the parent ductile iron and comparable to that of steel having hardness approximately twice that of the ADI. Sahin et al.[5] investigated the abrasive wear behavior of as-cast and ADIs with a dual-matrix structure subjected to different loads without any lubrication. They concluded that the wear resistance of the ADI with a dual-matrix structure was superior to that of the as-cast iron. Among the austempered samples, the lowest weight loss was observed for conventionally austempered samples, with a wholly ausferritic structure throughout the specimen, while the highest weight loss was obtained for the samples having the lowest ausferrite volume fractions in those samples with dual-matrix structures. Moreover, the wear resistance increased with an increasing ausferrite volume fraction and decreasing austempering time for all the tested samples. Yang et al.[30,31] studied the influence of the austempering temperature on the microstructure of ADI for a conventional single-step and a two-step process and its influence on the abrasion wear resistance. They concluded that the abrasion wear resistance of ADI decreases with an increase in the austempering temperature and the two-step austempering process gives a higher wear resistance for the ADI compared to the conventional single-step austempering process. The wear behavior of ADI has been found to be dependent on the material properties of the ADI, e.g., the yield strength, which are dependent on the microstructure.

Recent research by Cardoso et al.[32] evaluated the abrasive wear resistance of a group of different heat-treated nodular cast irons in comparison with white cast iron (WCI). In the wear resistance test, the WCI exhibited good performance due to its hardness. The ADI austempered at 573 K (300 °C) exhibited a performance slightly lower than the WCI during the initial period of the test. After a long exposure time to the abrasive material, the ADI austempered at 573 K (300 °C) exhibited a lower mass loss due to the constant transformation of the retained austenite into deformation-induced martensite. Sun et al.[33] compared the abrasion wear resistance of a new type of ductile cast iron containing carbide, known as CADI, to conventional ADI. The results showed that the abrasive wear resistance of the material was correspondingly enhanced

with the change in hardness, largely benefiting from the variations in the volume fraction and the size of the carbides. However, the improvement in the wear resistance due to the introduced hard carbides is generally accompanied by a decrease in the impact toughness, which limits its range of applications.

Putatunnda et al.[34] introduced a fully ferritic-structured ADI without compromising its mechanical and thermal properties. ADI with its ausferritic microstructure has very good combination of mechanical properties, but also it has some limitations. Austenite from ausferrite has a higher work hardening rate than ferrite[34–37] and this causes problems in the machining of ADI. Austenite–bainitic structure in ADI creates machinability and tool life problems because austenite is mechanically unstable and transforms to the martensite during machining. In addition, FCC austenite has a lower thermal conductivity than BCC ferrite, thus ADI has a relatively low thermal shock and thermal fatigue resistance because of mixed microstructure of ferrite and austenite. For example, brake rotors in automobiles and trucks need excellent thermal shock resistance, which in turn requires very high thermal conductivity. Another problem of austenite is that it has much higher coefficient of thermal expansion than ferrite, which can cause problems in applications where thermal fatigue is important.

In addition, there are several studies on the microstructure and properties of a new wear-resistant carbidic ADI where the carbide phase is introduced although the main characteristic of the ADI is that it has carbide-free austenite ferrite matrix.[38–42] The use of carbidic ADI is increasing because of its excellent combination of high abrasion resistance and good impact toughness compared to other materials with similar wear resistance.[43]

Research of deep cryogenic treatment on ADI started with the research of DCT on nodular cast iron. In the Reference 44 the results on the influence of DCT on ferritic–pearlitic nodular cast iron EN-GJS-600-3 were reported. The mechanical properties (tensile strength and impact toughness) and hardness were measured, also wear resistance, in the same manner as in this paper. There was no significant difference in the measured properties but wear resistance increased for approx. 15 pct. The tensile strength and impact toughness were measured on ADI after austempering process and the results were reported elsewhere.[45] Mechanical properties corresponded to the properties obtained when austempering in the upper bainitic range. Mechanical properties after cryogenic treatment reported by Panneerselvam et al.[46] slightly improves, both the yield and tensile strength for all austempering temperatures studied. Correspondingly, there was a decrease in the ductility of the ADI samples over the austempering temperature range. The results show that cryogenic treatment has little effect on the fracture toughness.

The purpose of this research was to investigate the influence of a deep cryogenic treatment on the abrasive wear resistance of ADI austempered in the upper ausferrite area since it was reported that upper ausferrite is more resistant to abrasive wear, as well as showing a greater thermal and mechanical stability of the high-carbon austenite compared to the lower ausferrite. In addition, the microstructural changes that occurred during the deep cryogenic treatment and the subsequent tempering were observed.

II. EXPERIMENTAL PROCEDURE

A. Material and Heat Treatment

The material used in this study was a pearlitic–ferritic nodular cast iron of grade EN-GJS-600-3. The test samples were cut from a Y-probe. The chemical composition of the nodular cast iron is given in Table I.

A quantitative analysis of the as-cast material's microstructure showed that it consists of around 130 graphite nodules per mm^2 and a bull's eye ferrite in a pearlitic matrix. The measured volume of pearlite was 62 pct, with the ferrite being 26 pct and the rest consisting of well-rounded graphite nodules. Mechanical properties of nodular cast iron were reported elsewhere.[45,47]

The heat treatments of the test samples were conducted in an electric furnace with a protective argon atmosphere. The test samples were austenitized at 1173 K (900 °C) for 90 minutes and then quenched to the austempering temperature of 673 K (400 °C). Subsequently, the samples were austempered for a period of 120 minutes at 673 K (400 °C) in salt bath AB1. Mechanical properties of ADI were reported and discussed elsewhere.[45] After the austempering the samples were slowly cooled to room temperature. The deep cryogenic treatment was performed by the controlled immersion of the individual test samples in nitrogen, where they were treated for 24 hours at a temperature of 77 K (−196 °C). The samples were then slowly heated to room temperature. Parts of the samples were then tempered at two different temperatures, i.e., 473 K and 623 K (200 °C and 350 °C), for a period of 2 hours and then slowly cooled to room temperature. Table II shows the sample groups (with the accompanying markings) and the conducted heat treatment. After the heat treatment a Vickers hardness of HV 30 was measured for all the test samples.

B. Microstructure Analyses

The samples for the microstructure analyses were taken for every heat-treatment condition. The samples were metallographically prepared using a standard procedure. For the optical microscopy the samples were etched with Klemm's tint etchant, while for the electron microscopy a solution of 2 pct Nital was employed. Klemm's tint etchant was used as a color etchant for the optical microscopy because it colors the ferrite phase, lightly colors the martensite and bainite, but does not react with the austenite. The microstructures of the samples were also analyzed with a FESEM JEOL JSM6500F field-emission scanning electron microscope using energy-dispersive X-ray spectroscopy (EDS), an INCA X-SGHT LN2-type detector, and an HKL

Percent C	Percent Si	Percent Mn	Percent P	Percent S	Percent Cu	Percent Mg	Percent Fe
3.57	2.49	0.113	0.029	0.007	0.4	0.057	balance

Table II. Markings on the Test Samples According to the Conducted Heat Treatment

Sample	Austenitization + Austempering	Deep Cryogenic Treatment	Tempering
ADI	1173.15 K (900 °C)/90 min, 673.15 K (400 °C)/120 min	—	—
DCT	1173.15 K (900 °C)/90 min, 673.15 K (400 °C)/120 min	77.15 K (−196 °C)/24 h	—
DCT1	1173.15 K (900 °C)/90 min, 673.15 K (400 °C)/120 min	77.15 K (−196 °C)/24 h	473.15 K (200°C)/2 h
DCT2	1173.15 K (900 °C)/90 min, 673.15 K (400 °C)/120 min	77.15 K (−196 °C)/24 h	623.15 K (350°C)/2 h
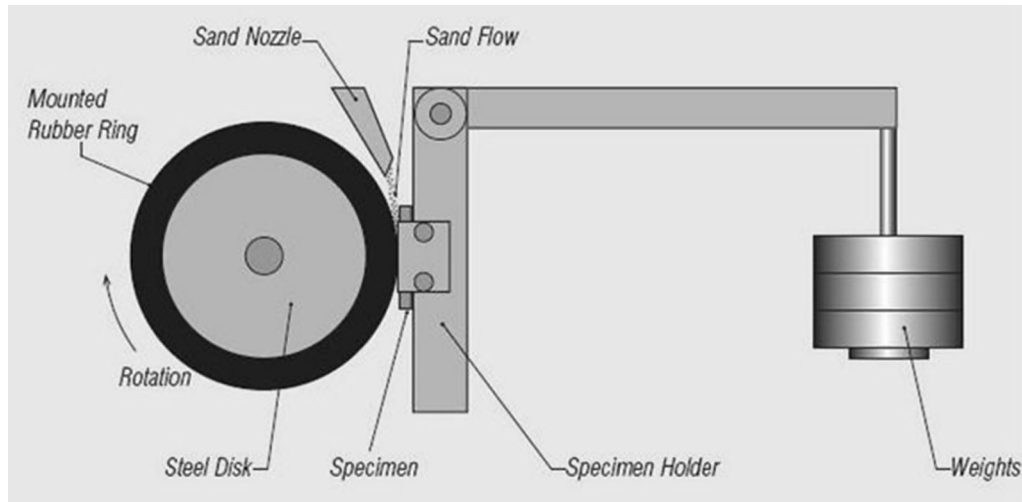
Fig. 1—"Dry sand/rubber wheel" test method in accordance with ASTM G65-94.

Nordlys II EBSD camera with Channel5 software. The EBSD mappings and the spot analyses were performed with samples tilted at 70.0 deg, using a 15 kV accelerating voltage and 1.5 nA probe current.

X-ray diffraction (XRD) (Panalytical XPert Pro PW3040/60) Cu-K$_\alpha$ radiation at 40 mA and 45 kV was used to identify the constituent phases of the ADI and the pure-iron controls with a scan range of 20 deg to 100 deg using a step size of 0.002 deg and a step time of 20 seconds. Narrow, more precise, measurements were performed with a scan range of 40 deg to 46 deg using a step size of 0.002 deg and a step time of 150 seconds. All the spectra were characterized with the software program X'Pert HighScore Plus, version 3.0a to obtain the peak positions and the integrated intensity of {111}, {220}, and {311} planes of FCC austenite and {110} and {211} planes of BCC ferrite. The volume fraction of austenite (X_γ) and ferrite (X_α) was determined by the direct comparison method using the integrated intensities of the above-mentioned planes by the following equation[48]:

$$\frac{I_\gamma(hkl)}{I_\alpha(hkl)} = \frac{R_\gamma(hkl)}{R_\alpha(hkl)} \cdot \frac{X_\gamma}{X_\alpha}, \quad [1]$$

where I_γ (hkl) is the integrated intensity from a given plane (hkl) of austenite phase (γ), I_α (hkl) is the integrated intensity from a given plane (hkl) of ferrite (α) phase, and R_γ (hkl) and R_α (hkl) are constants, where

$$R = \frac{1}{v^2\left(|F|^2 pL\right)e^{-2m}}, \quad [2]$$

where v is the atomic volume of unit cell, F is the structure factor, p is the multiplicity factor, L is the Lorentz–polarization factor, and e^{-2m} is the temperature factor.

The carbon content of austenite was determined by the equation[37]:

$$\alpha_\gamma = 0.3548 + 0.0044C_\gamma, \quad [3]$$

where α_γ is the lattice parameter of austenite in nanometer and C_γ the carbon content of austenite in wt pct. The {111}, {220}, and {311} planes of austenite were used to estimate the lattice parameter. Three samples were examined from every heat-treatment condition and the average from these samples is reported in this paper.
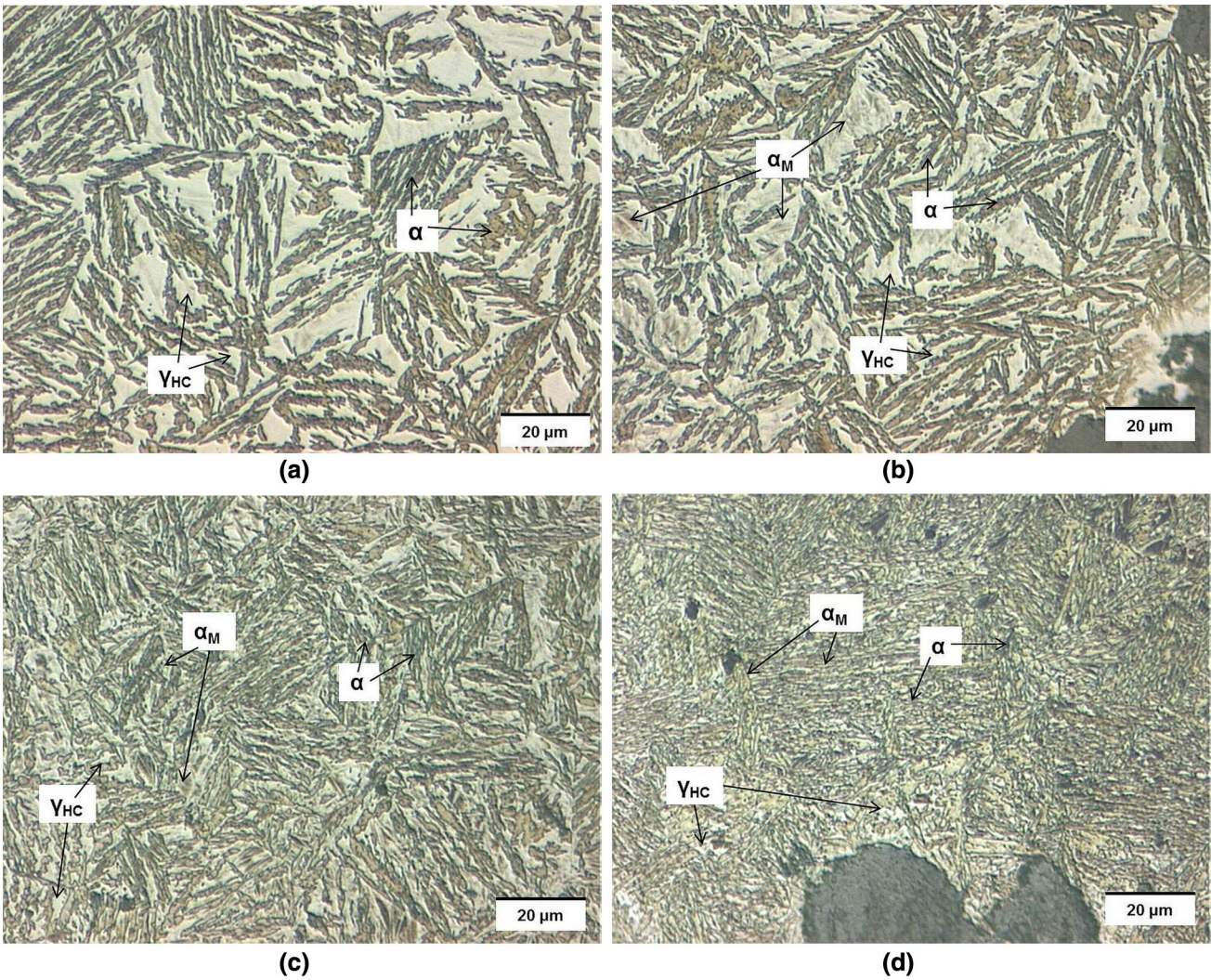
(a)   **(b)**

(c)   **(d)**

Fig. 2—Microstructure of (*a*) austempered ductile iron at 673.15 K (400 °C), (*b*) ADI deep cryogenic treated at 77.15 K (−196 °C)/24 h, (*c*) ADI deep cryogenic treated at 77.15 K (−196 °C)/24 h and tempered at 473.15 K (200 °C)/2 h, (*d*) ADI deep cryogenic treated at 77.15 K (−196 °C)/ 24 h and tempered at 623.15 K (350 °C)/2 h.
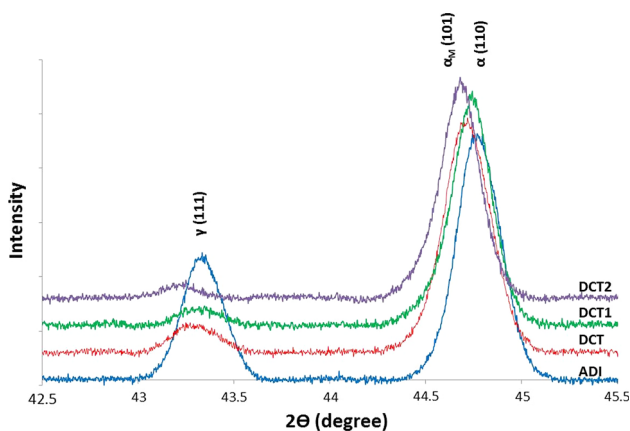

Fig. 3—X-ray patterns of tested samples.

For the EBSD analyses the samples were hot mounted in Bakelite, ground and polished with 3 and 1 μm diamond suspensions for 3 minutes at each stage. Next,
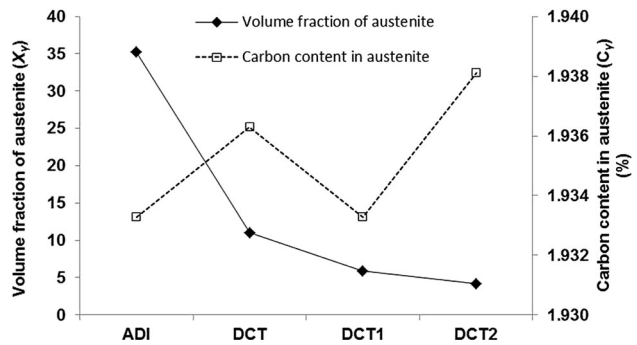
Fig. 4—Volume fraction of austenite and carbon content in austenite in tested samples.

the samples were cut to a thickness of 3 mm and polished using colloidal silica oxide (OPS commercial name of Struers). The polishing was performed manually, employing a very small force, at the rotating-disk speed of 300 revolutions per minute for 5 minutes. The
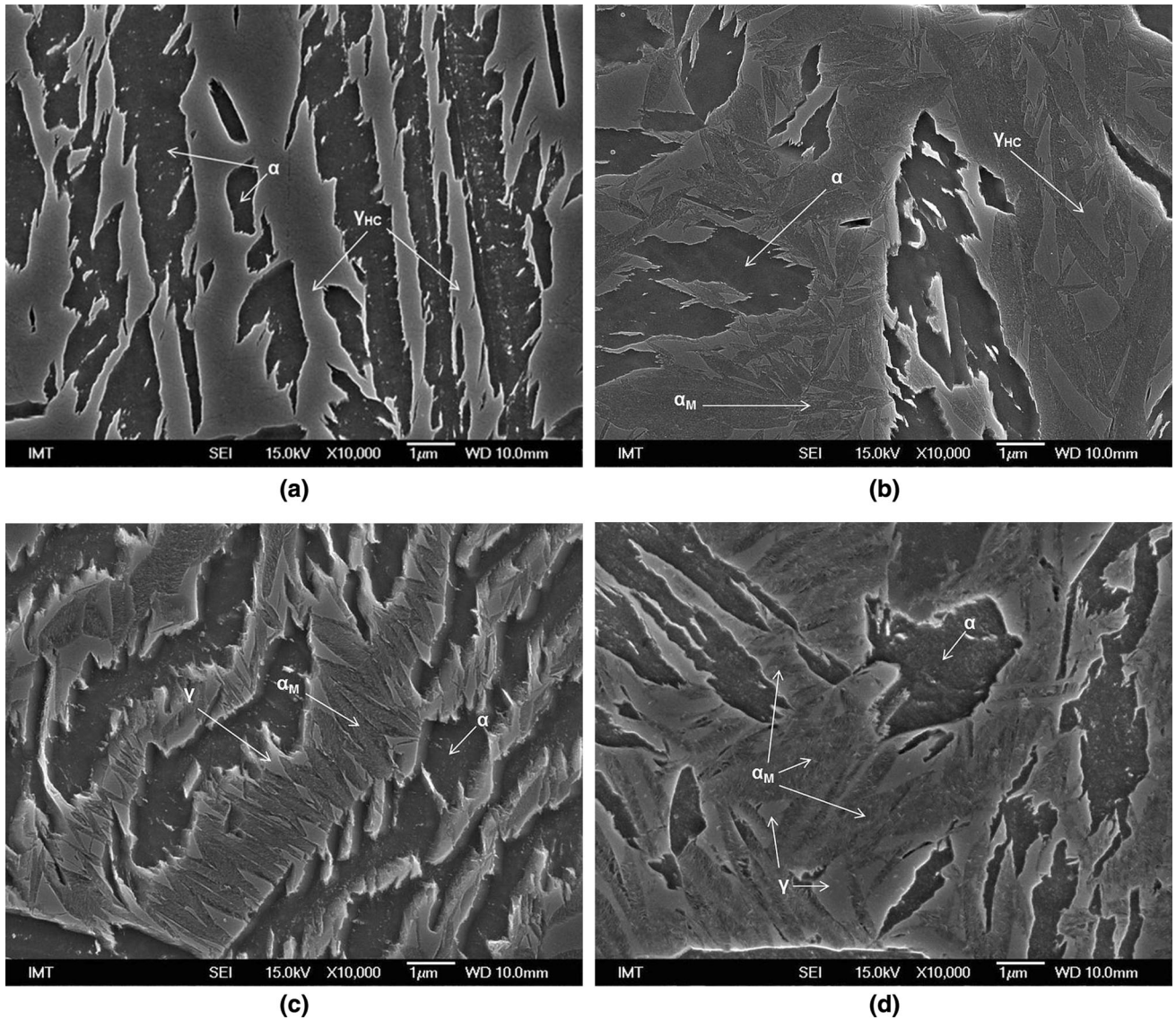
Fig. 5—FESEM microstructure of (*a*) austempered ductile iron at 673.15 K (400 °C), (*b*) ADI deep cryogenic treated at 77.15 K (−196 °C)/24 h, (*c*) ADI deep cryogenic treated at 77.15 K (−196 °C)/24 h and tempered at 473.15 K (200 °C)/2 h, (*d*) ADI deep cryogenic treated at 77.15 K (−196 °C)/24 h and tempered at 623.15 K (350 °C)/2 h.
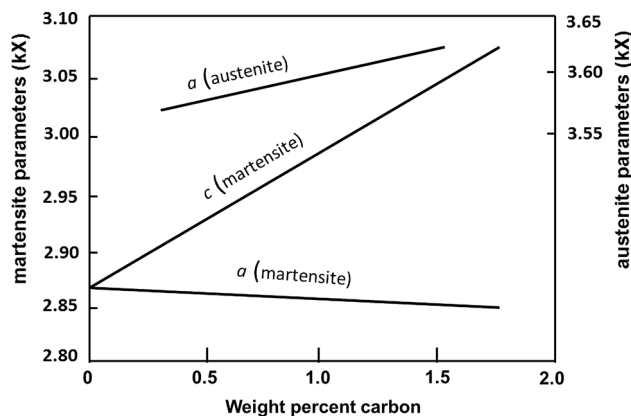

Fig. 6—Variation of the martensite and austenite lattice parameters with carbon content.

EBSD mappings were taken with a step size of 0.05 μm over an area of 12.35 × 10.05 μm^2. This technique uses crystallographic orientation mapping and crystallographic/lattice structural differences to provide information such as grain size measurements and distribution, boundary characteristics, crystallographic orientations and their distributions (or texture), and phase identification. EBSD is often used to obtain crystallographic information that is combined with optical microscopy or X-ray diffraction to better identify constituent phases. The EBSD analyses in this research was made to determine the martensite formation in the high-carbon austenite grains after the deep cryogenic treatment, since it was reported (as previously mentioned) that the austenite from the upper austempering temperature range has a great thermal stability, even if subjected to temperatures below the martensite finish temperature.
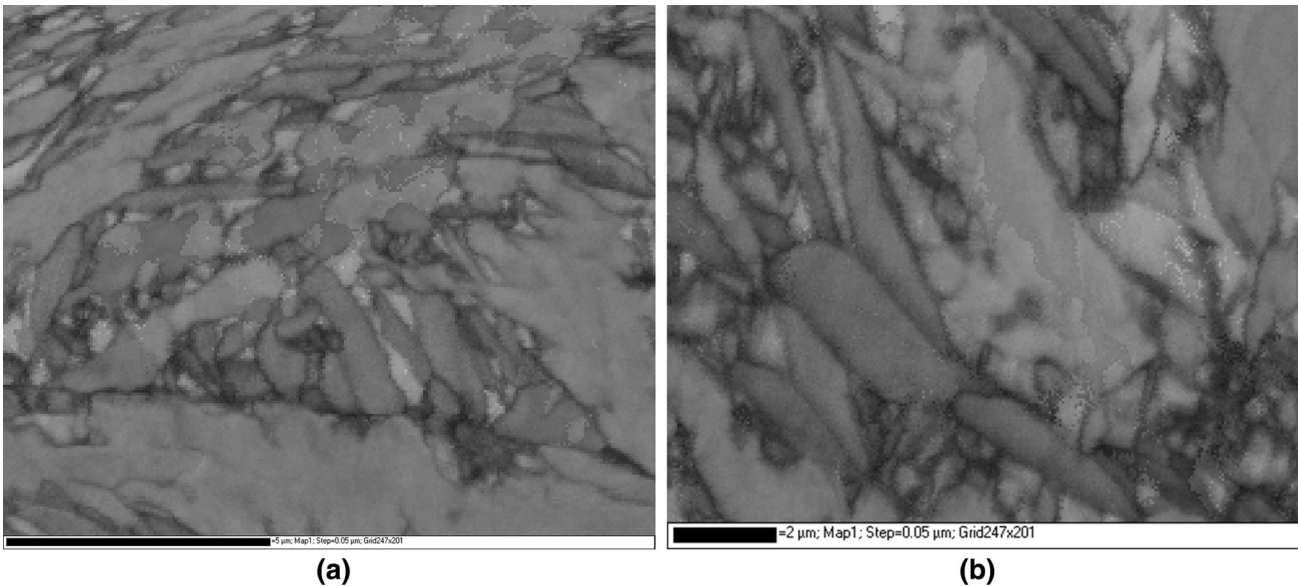
Fig. 7—Band-contrast image (*a*) Austempered ductile iron (ADI) sample, (*b*) Deep cryogenic-treated austempered ductile iron sample (DCT).
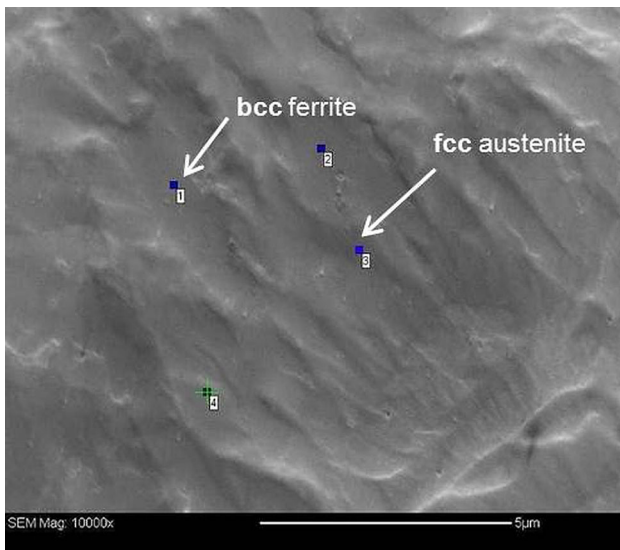

Fig. 8—SEI image of austempered ductile cast iron.

C. *Abrasion Wear Resistance*

The abrasion wear resistance was tested according to the standard ASTM G65-94 method "dry sand/rubber wheel." The test specimen, with dimensions of $75 \times 25 \times 15$ mm^3, was pressed against a rotating rubber wheel (hardness 60 Shore A) with a force of 130 N. The sand flow is directed into the gap between the wheel and the specimen, abrading the specimen under an applied normal load at a specific sliding speed (Figure 1).

The sand used as the abrasive was rounded silica sand Ottawa 50/70. The ASTM G65 standard was not exactly followed regarding the required number of the 6000 revolution because no other materials were compared to the material of this study; instead the abrasion wear was estimated according to the mass lost during the process.

The mass loss was measured after 100, 200, 500, 1000, and 2000 revolutions of the rubber wheel using a METLER B5C 1000 precision scale with a measuring range from 0 to 1000 g and within a tolerance of 0.0001 g as prescribed in the ASTM G65 standard. The relative wear resistance index, E_w, was obtained by the ratio between the volume loss experienced by a reference material (ΔV_R), (in this case a ADI sample) and by the deep cryogenic-treated samples (ΔV_S), according to Eq. [4].

$$E_w = \Delta V_R / \Delta V_S \qquad [4]$$

Volume loss was calculated from the mass loss using the density value measured for this ductile iron heat. Four wear tracks were made on every specimen and the results represent the mean value of four measurements. The testing was performed at room temperature and in an ambient laboratory atmosphere. The wear tracks were analyzed with a TESCAN Vega TS5136LS scanning electron microscope.

III. RESULTS AND DISCUSSION

The microstructures of the test samples after the conducted heat treatments are presented in Figure 2. Figure 2(a) shows the microstructure after the austempering process with a typical ausferritic matrix for the upper austempering range that consists of a dark-etched, coarse, feathery ferrite and a bright, unetched austenite. The microstructure after the deep cryogenic treatment at 77 K (−196 °C) for 24 hours is detailed in Figure 2(b). It is clear that the austenite transformed partially into martensite, but not completely. The formation of martensite needles is clearly visible in the austenite grains, but there is still much of the retained austenite present in the microstructure.
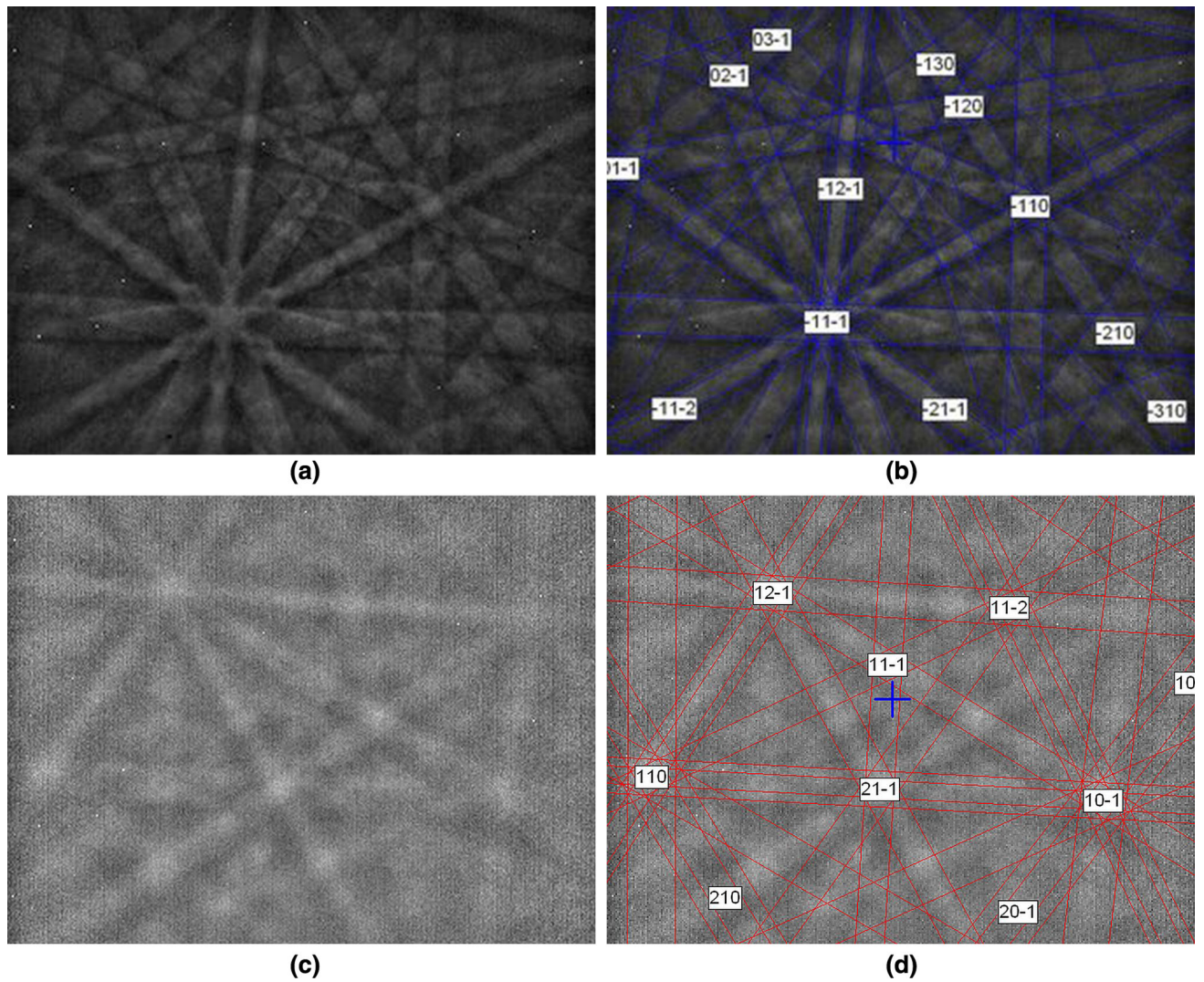
Fig. 9—(*a*) EBSD Kikuchi pattern of spot 1, (*b*) Indexed EBSD Kikuchi pattern of spot 1 as BCC ferrite, (*c*) EBSD Kikuchi pattern of spot 3, (*d*) Indexed EBSD Kikuchi pattern of spot 3 as FCC austenite.
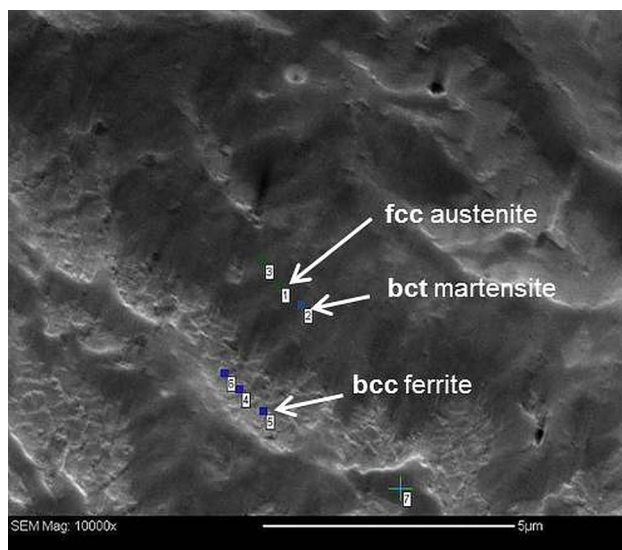

Fig. 10—SEI image of deep cryogenic-treated austempered ductile cast iron.

Figure 2(c) shows that the retained austenite is still present in the microstructure, but in smaller amounts. After 2 hours of tempering at 473 K (200 °C) the diffusion of the carbon from the austenite to the existing graphite nodules[34] partially decreased the amount of carbon in the retained austenite, so the martensite start temperature increased and the austenite with the lower carbon content became less stable and started to transform into martensite on cooling to room temperature.[49] The microstructure after tempering at 623 K (350 °C) is a fine-grained mixture of ferrite, martensite, and a small amount of high-carbon austenite. This also corresponds with the X-ray diffraction profiles of the samples, Figure 3, and the FESEM microstructure images in Fig 5. The volume fraction of austenite with its carbon content was determined by X-ray diffraction and the results are presented in Figure 4.

XRD pattern for deep cryogenic-treated samples (DCT) shows that austenite is still present after cooling the samples for 24 hours at 77 K (−196°C). The
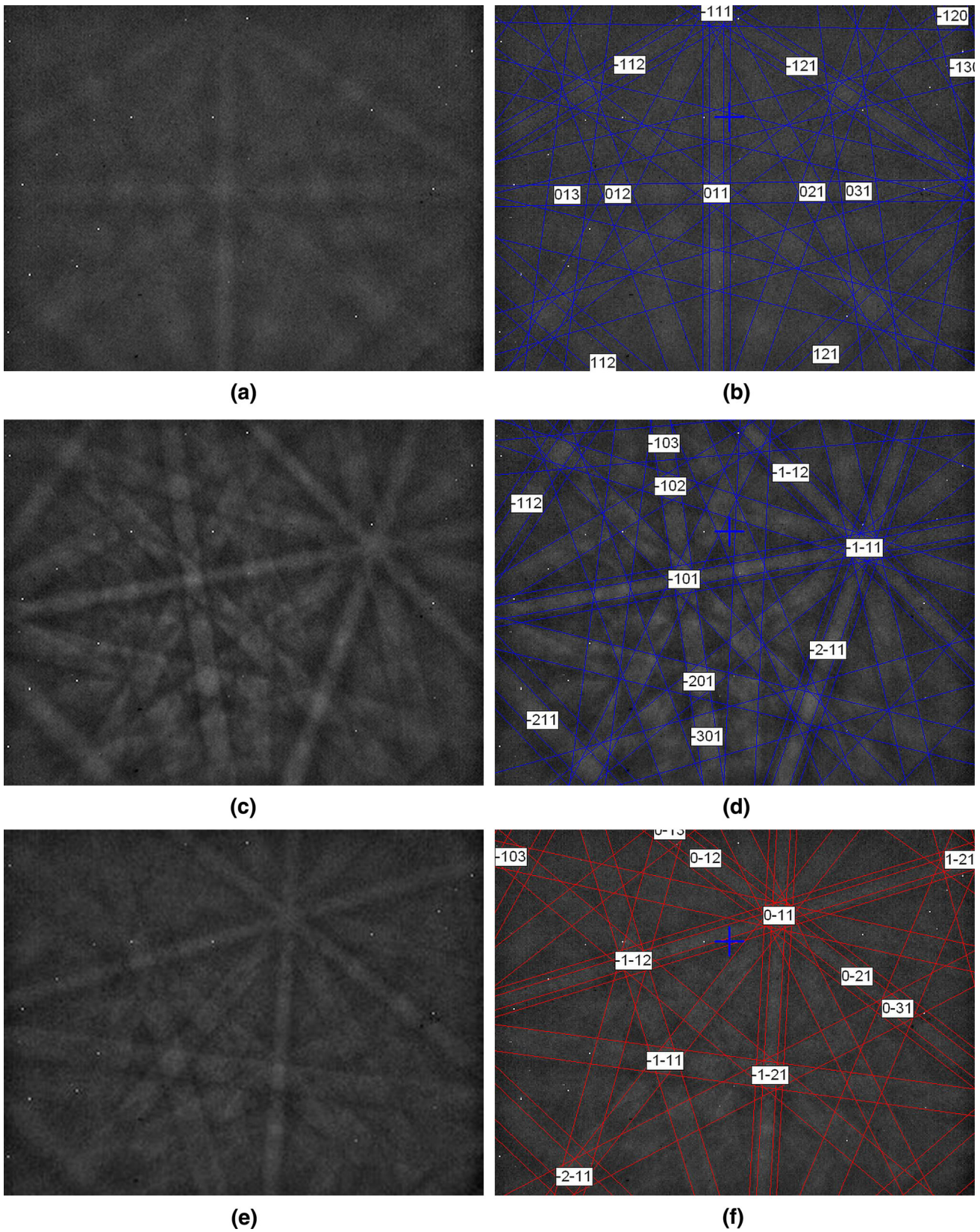
Fig. 11—Indexed EBSD Kikuchi pattern (*a*, *b*) spot 2, BCT martensite; (*c*, *d*) spot 1 BCC ferrite; (*e*, *f*) spot 5, FCC austenite.

widening of the peak indicates a smaller grain size with microstrain present in the austenite lattice.[48] It can be seen from Figure 4 that the volume fraction of the austenite decreased from approx. 35 to 11 pct with deep cryogenic treatment. This clearly indicates that the austenite from upper bainitic area is more thermally unstable when subjected to lower cryogenic temperature for longer period of time than reported in Reference 28.

It is clear that the austenite peak for the tempered samples at 623 K (350 °C) (DCT2) is shifted to the left, to lower angles, indicating an increase in the austenite lattice parameter due to the microstrain caused by the large amount of carbon. The martensite peak is also shifted to the left, which is in agreement with the change in the martensite and austenite lattice parameters with carbon content, as shown in Figure 6, based on Reference 48. The widening of the austenite peak with a lower intensity indicates a smaller austenite grain size as well as a decreased amount of austenite with tempering at higher temperature, in agreement with the results in Reference 31 and also with the results on Figure 4. The XRD patterns for the tempered samples did not indicate any large carbide formation during the tempering and there were no carbides observed in the microstructure during the optical and FESEM microscopy. No carbides were also observed in detailed analysis of the

microstructures using several different etchants including color etchants for revealing different microstructural phases and constituents; these results were published elsewhere.[45,47] It is possible that very fine carbides precipitated in the martensite during the subsequent tempering since no carbides were observed with metallographic methods used in this and other research which is in correlation with the literature.[15,18–22,26]

During the EBSD analysis, for each analyzing pixel the Kikuchi pattern quality was monitored, and then based on the band contrast a corresponding gray color was attributed by the software. Darker gray represents the area with worse band contrast; for instance, near the grain boundary the Kikuchi patterns are blurred due to two overlapping patterns. Different crystal orientations also lead to differences in the band contrasts. For certain crystal orientations a channeling effect occurred and fewer electrons are emitted. Such a band-contrast image represents a crystal structure with all the details, sometimes even better than using chemical etching. Different phases also have different band contrasts. Martensite is dark gray, while ferrite and austenite are lighter due to their clearer band contrasts in the Kikuchi patterns.

Figure 7 show band-contrast images in the austempered ductile iron (ADI) and after deep cryogenic treatment (DCT). It is clear that there are larger grains with subgrains of same orientations in the microstructure.

Figure 8 shows an SEI image of an ADI specimen with indications on the image where the EBSD spot analyses were performed. Figures 9(a) and (b) show the EBSD-indexed Kikuchi pattern for spot 1, characterized as the BCC crystal structure of ferrite. The sharp pattern indicates low strain in the crystal structure. Figures 9(c) and (d) show the EBSD-indexed Kikuchi pattern for spot 3, characterized as the FCC crystal structure of austenite. It can be seen that the Kikuchi pattern is not

Table III. Vickers Hardness HV 30, Relative Mass Loss, and Relative Volume Loss with Calculated Relative Wear Resistance E_w According to the Reference Sample ADI

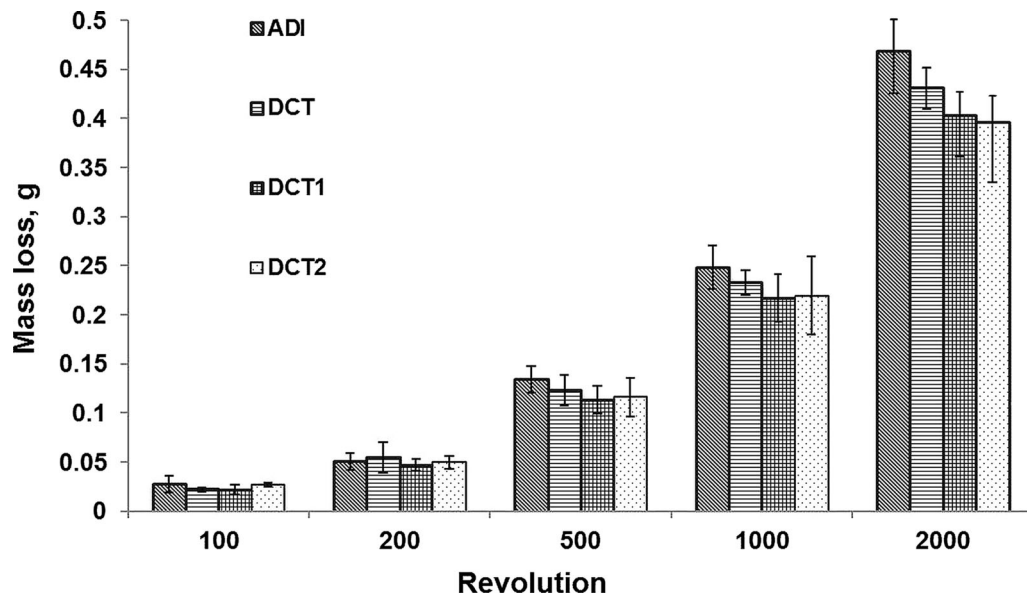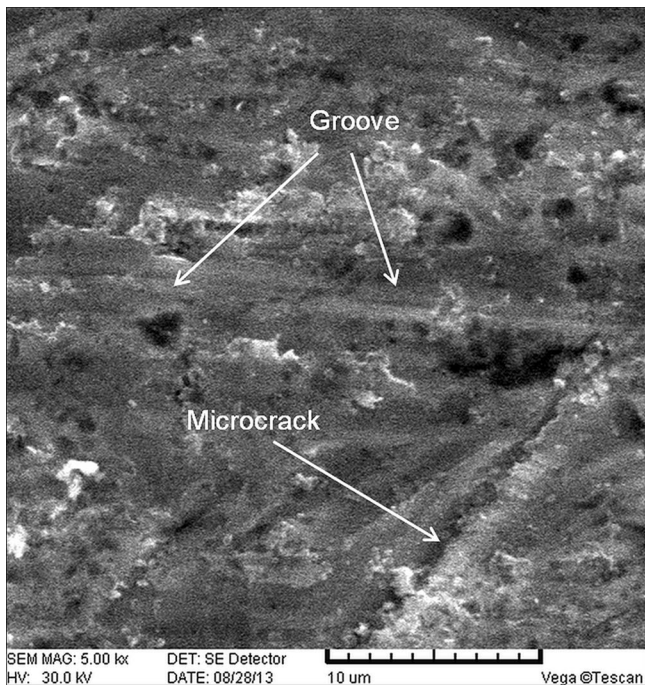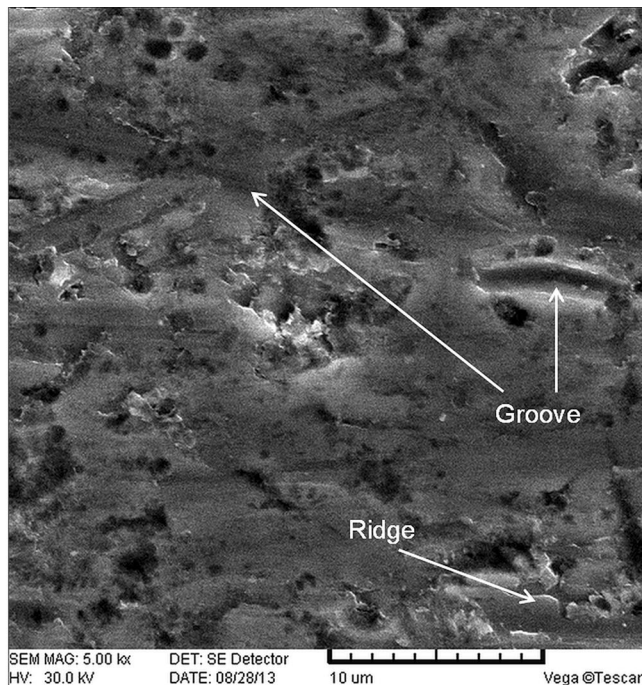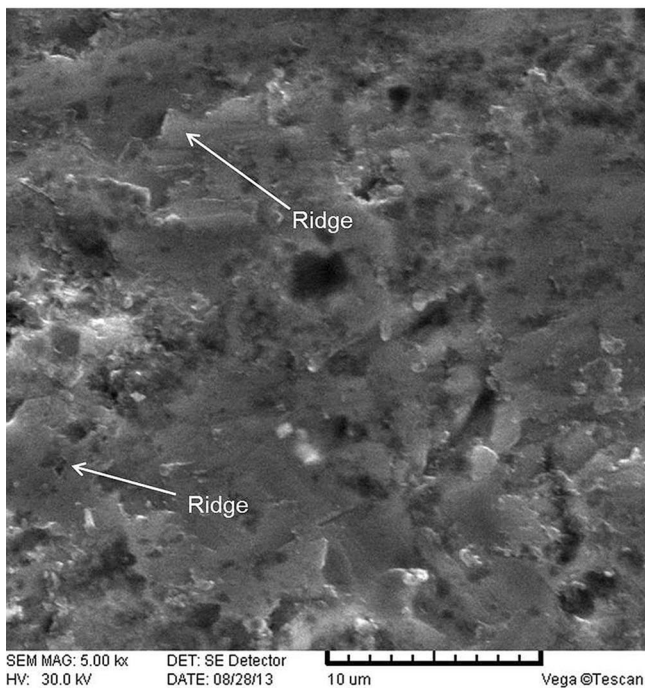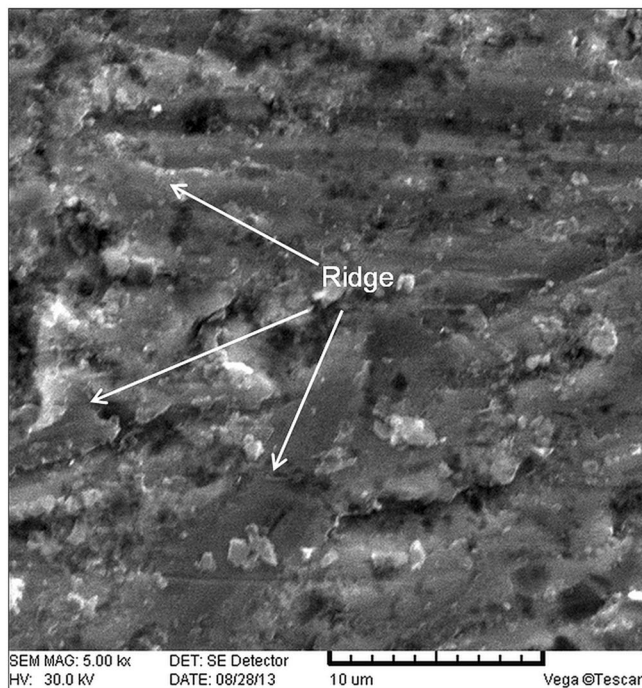|	Hardness, HV 30	Δm (g)	ΔV (cm^3)	Ew
ADI	296 ± 2.01	0.469	3.327	1
DCT	309 ± 2.11	0.431	3.057	1.088
DCT1	330 ± 2.12	0.403	2.857	1.164
DCT2	390 ± 1.56	0.397	2.816	1.182

Fig. 12—Mass loss during the abrasion wear testing.

Fig. 13—SEM images of abrasion wear tracks: (a) austempered ductile iron at 1173.15 K (900 °C)/90 min, 673.15 K (400 °C)/120 min, (b) ADI deep cryogenic treated at 1173.15 K (900 °C)/90 min, 673.15 K (400 °C)/120 min, 77.15 K (−196 °C)/24 h, (c) ADI deep cryogenic treated at 1173.15 K (900 °C)/90 min, 673.15 K (400 °C)/120 min, 77.15 K (−196 °C)/24 h and tempered at 473.15 K (200 °C)/2 h, (d) ADI deep cryogenic treated at 1173.15 K (900 °C)/90 min, 673.15 K (400 °C)/120 min, 77.15 K (−196°C)/24 h and tempered at 623.15 K (350 °C)/2 h.

sharp. The blurred pattern is the result of high stress in the crystal structure, which is caused by the large amount of carbon dissolved in the austenite.

Figure 10 shows an SEI image of deep cryogenic-treated ADI with marked spots where the EBSD spot analyses were performed. Figures 11(a) and (b) show the EBSD-indexed Kikuchi pattern of spot 2, characterized as the BCC/BCT crystal structure of martensite; however, due to the large strain in the martensitic crystal structure the pattern is very blurred.

Figures 11(c) and (d) show the EBSD-indexed Kikuchi pattern of spot 5, characterized as the BCC crystal structure of ferrite, and the sharp pattern represents less strain in the crystal structure than in the martensite in spot 2.

Figures 11(e) and (f) show the EBSD-indexed Kikuchi pattern of spot 1, characterized as the FCC crystal structure of austenite. The austenite Kikuchi pattern of the DCT specimen is also visibly more blurred than FCC pattern in ADI sample, representing more strain in the austenite crystal structure which corresponds with XRD analysis which showed that deep cryogenic treatment reduced the amount of austenite for more than 20 pct but the carbon content in the austenite has increased which caused more microstrain of the austenite lattice.

A Vickers hardness of HV 30 was measured on all the samples after the heat treatment. The results are shown in Table III, and they represent the mean value of ten measurements made on three samples for every conducted heat-treatment procedure.

The results show that the deep cryogenic treatment did not significantly influence the hardness of the austempered ductile iron, although the amount of austenite reduced from 35 to 11 pct. Tempering after the deep cryogenic treatment contributed, in a statistically significant way, to the increase in the hardness that corresponds with the microstructure analysis and the martensite formation during the deep cryogenic treatment and cooling after subsequent tempering and with possible ultrafine carbide precipitation during tempering.[49]

The results of the abrasion wear testing show that the deep cryogenic treatment has an influence on the mass loss of the tested specimens and the results are presented in Figure 12. Relative mass loss and relative volume loss with calculated relative wear resistance E_w according to the reference sample ADI are presented also in Table III. Table III shows that deep cryogenic-treated specimens showed an approximately 16 and 18 pct, respectively better abrasive wear resistance compared to the nontreated ADI.

The results show that all the cryogenic-treated specimens had a lower mass loss than the ADI specimens. Both groups of cryogenic-treated and tempered samples (DCT1 and DCT2) had approximately the same mass loss, although the specimens tempered at the higher tempering temperature of 623 K (350 °C) had a 20 pct higher hardness. The similar results were obtained on deep cryogenic-treated nodular cast iron where 15 pct lower mass loss was obtained compared to the untreated nodular cast iron, without change in hardness and without any visible changes in microstructure.[47] Although the higher hardness is usually corresponding to higher wear resistance, many studies have clearly demonstrated that the simple correlation of abrasion resistance and hardness does not always hold true.[50–54] The results of several investigations on tool steels shows that hardness of a tool steel is mainly influenced by retained (soft) austenite and in this way deep cryogenic treatment can play an important role. However, when compared to wear results, hardness test results indicate

that the mechanisms can be different for different materials.[26] For instance Molinari et al. presented in Reference 55 an +0.13 pct increase in hardness with deep cryogenic treatment that has induced a 51 pct decrease in wear rate for AISI M2 and the authors have concluded that AISI M2 wear resistance improvement can be attributed to hardness increase. The same test on AISI H13 tool steel has shown an improvement of 6.9 pct in hardness related to a decrease of 29 pct in wear rate and, according to the authors, the wear resistance improvement has been correlated to the enhanced toughness of the cryogenically treated material.

The analysis of the abrasion wear tracks showed the presence of both mild and severe abrasion mechanisms of microplowing and microcutting, Figure 13. The wear tracks are grooved and considerably roughened, and besides the plastically deformed areas, where a certain fraction of the grooved material is just shifted to the edges of the rim as a result of microplowing, grooves with different depths and pits can be seen on all samples. The grooves are deeper in the first two samples (ADI and DCT), Figures 13(a) and (b), which correspond with the lower hardness measured on these samples, where the microcutting mechanism is also more pronounced due to the larger amount of relatively soft microstructural phases, in agreement with the literature.[56–61]

IV. CONCLUSIONS

The influence of a deep cryogenic treatment in combination with tempering on the microstructure and abrasion wear resistance was examined. The results showed that the austenite formed at the upper austempering temperature of 673 K (400 °C) C is not as thermally stable when subjected for 24 hours to the liquid nitrogen temperature of 77 K (−196 °C) as reported in Reference 28, where the samples were cryogenically treated at −123 K (−150 °C) for 4 hour. The amount of austenite reduced from 35 to 11 pct with 24 hours deep cryogenic treatment. The hardness and abrasion wear resistance after deep cryogenic treatment increased due to the martensite formation.

The subsequent tempering at both temperatures contributed to the increase of the hardness and to the abrasion wear resistance due to the possible precipitation of ultrafine carbides in the martensite during tempering. The analysis of the abrasion wear tracks showed the presence of the combined mechanisms of mild and severe abrasion, which were more visible on the deep cryogenic-treated samples.

The deep cryogenic-treated samples showed an approximately 10 to 18 pct better abrasion wear resistance, while both groups of cryogenic-treated and tempered samples had approximately the same mass loss, although the specimens tempered at the higher tempering temperature had a 20 pct higher hardness.

Although there has not been much research on the influence of deep cryogenic treatments on the microstructure and properties of austempered ductile

iron, the results from this research combined with the literature data indicate that it has a positive influence on both the wear resistance and the hardness. Since a cryogenic treatment is a relatively simple procedure that can be easily implemented in the heat-treatment process, further research should be conducted to investigate more possibilities for improving the mechanical and tribological properties of ADI.

REFERENCES

1. V. Kilicli and M. Erdogan: *Int. J. Cast Met. Res.*, 2007, vol. 20, pp. 202–14.
2. M. Ferry and W. Xu: *Mater. Charact.*, 2004, vol. 53, pp. 43–49.
3. A. M. Kamshushi, Doctoral thesis, University of Malta, 2005.
4. T Tun and KT Lwin: *J. Met. Mater. Miner.*, 2008, vol. 18 (2), pp. 199–205.
5. Y. Sahin, M. Erdogan, and V. Kilicli: *Mater. Sci. Eng., A*, 2007, vol. 444, pp. 31–38.
6. C.Z. Wu, Y.J. Chen, and T.S. Shih: *Mater. Charact.*, 2002, vol. 48, pp. 43–54.
7. J.M. Han, Q. Zou, G.C. Barber, T. Nasir, D.O. Northwood, X.C. Sun, and P. Seaton: *Wear*, 2012, vols. 201–201, pp. 99–105.
8. B. Radulovic and B. Bosnjak: *Mater. Tehnol.*, 2000, vol. 35 (5), pp. 207–12.
9. L. Sidjanin and R.E. Smallman: *Mater. Sci. Technol.*, 1992, vol. 8, pp. 1095–1103.
10. W.J. Dubensky and K.B. Rundman: *AFS Trans.*, 1985, vol. 93, pp. 389–94.
11. D.J. Moore, T.N. Rouns, K.B. Rundamn, J. Heat Treat. 4, 1985, vol. 1, pp. 7–24.
12. D.N. Collins: *Adv. Mater. Process.*, 1998, vol. 154 (6), pp. H23–H29.
13. D. Mohan Lal, S. Renganarayanan, and A. Kalanidhi: *Cryogenics*, 2001, vol. 41, pp. 149–55.
14. A. Molinari, M. Pellizzari, S. Gialanella, G. Straffelini, and K.H. Stiasny: *J. Mater. Process. Technol.*, 2001, vol. 118, pp. 350–55.
15. R.F. Barron: *Cryogenics*, 1982, vol. 22, pp. 409–14.
16. P.J. Singh, S.L. Mannan, T. Jayakumar, and D.R.G. Achar: *Eng. Fail. Anal.*, 2005, vol. 12, pp. 263–71.
17. B. Podgornik, F. Majdic, V. Leskovsek, and J. Vizintin: *Wear*, 2012, vol. 288, pp. 88–93.
18. A. Bensely, A. Prabhakaran, D. Mohan Lal, and G. Nagarajan: *Cryogenics*, 2006, vol. 45, pp. 747–54.
19. F. Meng, K. Tagashira, R. Azuma, and H. Sohma: *ISIJ Int.*, 1994, vol. 34, pp. 205–10.
20. S. Šolić, F. Cajner, and P. Panjan: *Materialwiss. Werkstofftech.*, 2013, vol. 44 (12), pp. 950–58.
21. S. Šolić, F. Cajner, V. Leskovšek, and M.P. Mat: *Test*, 2012, vol. 2012 (10), pp. 688–93.
22. P.F. Stratton, IFHTSE 2005. Pula, pp. 11–19.
23. H.S. Yang, J. Wang, B.L. Shen, H.H. Liu, S.J. Gao, and S.J. Huang: *Wear*, 2006, vol. 261, pp. 1150–54.
24. T. Slatter, R. Lewis, and A.H. Jones: *Wear*, 2011, vol. 271, pp. 1481–89.
25. R. Thornton, T. Slatter, A.H. Jones, and R. Lewis: *Wear*, 2011, vol. 271, pp. 2386–95.
26. P. Baldissera and D. Delprete: *Open Mech. Eng. J.*, 2008, vol. 2, pp. 1–11.
27. S. Putatunda, C. Martis, R. Papp, and F. Diekman: Proceedings of the 26th ASM Heat Treating Society Conference, 2011, pp. 44–49.
28. S. Panneerselvam, C.J. Martis, S.K. Putatunda, and J.M. Boileau: *Mater. Sci. Eng., A*, 2015, vol. 626, pp. 237–46.
29. J. Zimba, D.J. Simbi, and E. Navara: *Cem. Concr. Compos.*, 2003, vol. 25, pp. 643–49.
30. J. Yang and S.K. Putatunda: *Mater. Sci. Eng., A*, 2005, vol. 406, pp. 217–28.
31. J. Yang and S.K. Putatunda: *Mater. Des.*, 2004, vol. 25, pp. 219–30.
32. P.H.S. Cardoso, C.L. Israel, and T.R. Strohaecker: *Wear*, 2014, vol. 313, pp. 29–33.
33. X. Sun, Y. Wang, D.Y. Li, and G. Wang: *Wear*, 2013, vol. 301, pp. 116–21.
34. S.K. Putatunda, S. Kesani, R. Tackett, and G. Lawes: *Mater. Sci. Eng., A*, 2006, vols. 435–436, pp. 112–22.
35. R.E. Reed Hill: *Physical Metallurgy Principles*, 2nd ed., D. Van Nostrand Company, New York, 1973.
36. D.A. Porter and K.E. Easterling: *Phase Transformations in Metals and Alloys*, 2nd ed., Chapman & Hall, New York, 1992.
37. W.F. Smith: *Structure and Properties of Engineering Alloys*, McGraw-Hill, New York, 1981.
38. P.Y. Cheng, J. Hui-Jin, L. Jin-Hai, and L. Guo-Lu: *Mater. Charact.*, 2012, vol. 72, pp. 53–58.
39. S. Laino, J.A. Sikora, and R.C. Dommarco: *Wear*, 2008, vol. 265, pp. 1–7.
40. A.A. Nofal and L. Jekova: *J. Univ. Chem. Technol. Metall.*, 2009, vol. 44 (3), pp. 213–28.
41. A.K. Chowdhury, S.K. Samanta, D.P. Chattopadhyay, S. Kumar, T. Ray, and S.S. Sinha: Roy*Indian Foundry J.*, 2009, vol. 55 (8), pp. 23–31.
42. S. Laino and J.A. Sikora: R.C. Dommarco*ISIJ Int.*, 2009, vol. 49 (8), pp. 1239–45.
43. S. Laino, J.A. Sikora, and R.C. Dommarco: *ISIJ Int.*, 2009, vol. 49 (8), pp. 1239–45.
44. S. Šolić and S. Jakovljević: Proceedings of the EWF EUROJOIN 8 Conference, 2012, pp. 91–98.
45. S. Šolić, Z. Schauperl, and S. Jakovljević: Book of abstracts, 20th International Conference on Materials and Technology, 2012, p. 215.
46. S. Panneerselvam, C.J. Martis, S.K. Putatunda, and J.M. Boileau: *Mater. Sci. Eng., A*, 2015, vol. 626, pp. 237–46.
47. S. Šolić, Z. Schauperl, and M. Godec: Proceedings Book of 13th International Foundrymen Conference, 2013, pp. 395–403.
48. B.D. Cullity: *Elements of X-ray Diffraction*, Addison-Wesley, Reading, MA, 1974, pp. 391–95.
49. G. Roberts, R. Kennedy, and G. Krauss: Tool Steels, 5th edition, ASM, 1998, pp. 99–101.
50. X. Xiaojun, W. Xu, F.H. Ederveen, and S. van der Zwaag: *Wear*, 2013, vol. 301, pp. 89–93.
51. B. Narayanaswamy, P. Hodgson, and H. Beladi: *Wear*, 2016, vols. 350–351, pp. 155–65.
52. K.H.Z. Gahr: *Microstructure and Wear of Materials*, Elsevier Science Ltd., Amsterdam, 1987.
53. P.J. Mutton and J.D. Watson: *Wear*, 1978, vol. 48, pp. 385–398.
54. L.Q. Xu and N.F. Kennon: *Wear*, 1991, vol. 148, pp. 101–12.
55. A. Molinari, M. Pellizzari, S. Gialanella, G. Straffelini and K. H. Stiasny: Proceedings of Conference on Advances Materials Processes Technologies, 1999, pp. 1461–69.
56. M.R. Berrahmoune, S. Berveiller, K. Inal, A. Moulin, and E. Patoor: *Mater. Sci. Eng., A*, 2004, vol. 378, pp. 304–07.
57. J.D. Gates: *Wear*, 1998, vol. 214, pp. 139–46.
58. M.M. Kruschov: *Wear*, 1974, vol. 28, pp. 69–88.
59. R.C.D. Richardson: *Wear*, 1968, vol. 11, pp. 245–345.
60. R.A. Martínez: *Eng. Fract. Mech.*, 2010, vol. 77, pp. 2749–62.
61. G. Francucci, J. Sikora, and R. Dommarco: *Mater. Sci. Eng., A*, 2008, vol. 485, pp. 46–54.